The Journal of Chemical Physics

Isotope effects on the structural transformation and relaxation of deeply supercooled water

Cite as: J. Chem. Phys. **156**, 084501 (2022); https://doi.org/10.1063/5.0078796
Submitted: 15 November 2021 • Accepted: 01 February 2022 • Accepted Manuscript Online: 01 February 2022 • Published Online: 22 February 2022

Loni Kringle, Wyatt A. Thornley, Bruce D. Kay, et al.

The Journal of Chemical Physics ARTICLE scitation.org/journal/jcp

Isotope effects on the structural transformation and relaxation of deeply supercooled water

Cite as: J. Chem. Phys. 156, 084501 (2022); doi: 10.1063/5.0078796
Submitted: 15 November 2021 • Accepted: 1 February 2022 •
Published Online: 22 February 2022

Loni Kringle,[a] Wyatt A. Thornley, Bruce D. Kay, and Greg A. Kimmel

AFFILIATIONS

Physical Sciences Division, Pacific Northwest National Laboratory, P.O. Box 999, Richland, Washington 99352, USA

Note: This paper is part of the JCP Special Topic on Slow Dynamics.
[a]**Author to whom correspondence should be addressed:** loni.kringle@pnnl.gov

ABSTRACT

We have examined the structure of supercooled liquid D_2O as a function of temperature between 185 and 255 K using pulsed laser heating to rapidly heat and cool the sample on a nanosecond timescale. The liquid structure can be represented as a linear combination of two structural motifs, with a transition between them described by a logistic function centered at 218 K with a width of 10 K. The relaxation to a metastable state, which occurred prior to crystallization, exhibited nonexponential kinetics with a rate that was dependent on the initial structural configuration. When the temperature is scaled by the temperature of maximum density, which is an isostructural point of the isotopologues, the structural transition and the non-equilibrium relaxation kinetics of D_2O agree remarkably well with those for H_2O.

I. INTRODUCTION

Although water is ubiquitous, a great deal remains to be understood about the origin of its anomalous properties. Progress has been made with theory and molecular dynamics (MD) simulations, with growing consensus that water's anomalies are related to the presence of two liquid structural forms, typically referred to as high-density liquid water (HDL) and low-density liquid water (LDL).[1–6] However, water's rapid crystallization in the supercooled temperature regime has limited the experimental investigation where leading models predict key phenomena occur. Therefore, the behavior of real water is still debated.

New experimental techniques have pushed the limits imposed by rapid crystallization to examine water's previously inaccessible temperature regime in different ways including rapid evaporative cooling of micrometer sized droplets,[7,8] nanoconfinement,[9] and ultrafast heating and decompression methods.[10] Using a pulsed laser to transiently heat nanoscale water films in nanosecond increments,[11,12] we recently showed that H_2O undergoes reversible transitions between two structural motifs at temperatures between 135 and 245 K.[13] We have also examined the dynamic behavior of the associated changes in the molecular configurations, as probed by infrared spectroscopy, as supercooled water relaxes toward a structurally equilibrated metastable supercooled liquid prior to crystallization.[14] In this work, we apply the pulsed laser heating technique to the study of D_2O, to examine the role of isotope effects at deeply supercooled temperatures.

While the isotope effects of many molecular liquids can be described by classical mass effects,[15] these models fail to explain the temperature dependent behavior of water and heavy water.[16] Likewise, the van der Waal's theorem of corresponding states,[17] which postulates that fluids have approximately the same equation of state when scaled by their liquid–gas critical temperature, T_C, and pressure, P_C, not only fails but also predicts the opposite behavior. The divergence from these models is typically attributed to the role of nuclear quantum effects (NQEs), such as the zero-point energy, proton delocalization, and tunneling.[18] While MD simulations with flexible water models have demonstrated the competition of quantum effects,[18–20] the role of NQEs is generally considered to strengthen the hydrogen bonding network of D_2O resulting in a more tetrahedrally bonded liquid.[18]

In 1986, Root *et al.* investigated the structural differences between H_2O and D_2O at 297 K using γ-ray diffraction.[21] It has since been proposed that to accurately examine the H/D isotope effects, it is useful to examine H_2O and D_2O when their liquid structures are equivalent, which is not necessarily at the same temperature. A common approach to facilitate this was developed by Robinson and co-workers, which they referred to as the thermal offset conjecture.[22] They used a two state model to argue that the structural properties of H_2O are equivalent to those of D_2O at an elevated temperature

[i.e., $T(D_2O) = T(H_2O) + \delta$, where δ is the effective offset]. Over time, δ has evolved to become a fitting parameter and has been successfully applied to dynamic and thermodynamic properties with a value typically between the difference in melting temperature [$\Delta T_m = T_m(D_2O) - T_m(H_2O) = 3.8$ K] and the difference in temperature of maximum density [$\Delta T_{MD} = T_{MD}(D_2O) - T_{MD}(H_2O) = 7.2$ K],[8,22–30] with some notable exceptions.[31,32]

An alternative approach, which removes the fitting of δ, is to scale the temperature by that of a known isostructural point, such as the temperature of maximum density (T_{MD}). This alternative corresponding states argument was put forth by Limmer and Chandler to compare different classical interaction potential models used in MD simulations.[33] They argued that the variability of the location of specific features within the water phase diagram for the models is a manifestation of the delicate balance between energy and entropy and that the emergence of a point of maximum density is a direct result of this energy–entropy balance.[33] The isotope effects are also impacted by this balance, leading to the 7.2 K increase in T_{MD} upon H/D substitution.[18] When applied to H_2O and D_2O, this approach leads to results similar to that of the thermal offset conjecture near T_{MD}. However, the magnitude of the isotope effect changes linearly with temperature in this scenario, whereas the thermal offset conjecture is temperature independent.

In this work, we investigate the steady-state structural composition of supercooled D_2O at temperatures between 185 and 255 K, where the liquid structure is expected to be rapidly changing, yet little experimental data exists. We find that prior to the onset of crystallization, the structure can be reproduced by a linear combination of two structural motifs typical of liquid D_2O at high and low temperatures. We also investigate the structural relaxation kinetics for D_2O prepared in two different initial configurations as it approaches steady state. When compared isostructurally to H_2O, we find excellent agreement in the structural composition and effective relaxation times of the two isotopologues.

II. EXPERIMENTAL DETAILS

Samples of D_2O with a coverage of 50 monolayers (ML) were deposited at normal incidence onto a Pt(111) or graphene/Pt(111) substrate held at 70 K in ultra-high vacuum ($<10^{-10}$ Torr) using molecular beam dosing techniques to prepare a non-porous, amorphous solid water (ASW) film.[34–36] A coverage of 1 ML corresponds to $\sim 1 \times 10^{19}$ molecules/m^2 and for densities of ~1.1 g/cm^3, a 50 ML D_2O film should be ~15 nm thick.

The nanoscale D_2O films were transiently heated to intermediate temperatures using a pulsed laser heating technique, which has been described in detail previously.[11] Briefly, a laterally homogeneous, infrared laser pulse (Nd:YAG, $\lambda = 1064$ nm, full width at half maximum ~10 ns) is absorbed in the near surface region of the substrate and the ensuing heat transfer transiently heats and subsequently cools the D_2O sample at rates of $\sim 10^{10}$ and $\sim 5 \times 10^9$ K/s, respectively.[11] T_{max} is calibrated from the measured desorption rate of crystalline ice (CI) during the pulsed heating[11] and the known vapor pressure of ice.[37,38] Small lateral heterogeneities in the laser pulse energy (i.e., an imperfect flat top profile) produce lateral variations in the temperature of the water films. Using the higher desorption rate from these laser "hot spots,"[11] the lateral temperature variations are estimated to be ±3 K for the temperature range relevant to the current experiments. Furthermore, the ability to reproducibly set the laser pulse energy with the variable attenuator results in small variations in T_{max}, as determined from the reproducibility of the temperature calibration measurements. The temperature, $T(z,t)$, in the substrate and water film vs time, t, and distance normal to the substrate, z, was calculated by solving the one-dimensional heat transfer equation. For the experiments reported here, the differences in $T_{max}(z)$ within the water film were <3 K.[11,12]

For thicker films, the time constant for transferring heat into the outer portions of the water film increases relative to the time needed to dissipate the heat pulse into the metal substrate, thus limiting the ability to uniformly heat the water films.[39] As a result, experiments on substantially thicker films are not feasible with the current approach. For H_2O, the results of control experiments with coverages between 20 and 100 ML films were qualitatively similar to those on 50 ML films and also consistent with the expected changes in $T(z,t)$ for films with these thicknesses.[13] Because most molecular dynamics simulations indicate that the properties of water converge to the bulk within a few monolayers of an interface,[40,41] even for supercooled water,[42] we believe that the current results are representative of bulk water. Furthermore, because the maximum correlation length for water at low pressures is <0.5 nm,[8] we also do not expect the density fluctuations in our supercooled water films to be strongly perturbed relative to the bulk. However, we cannot rule out possible influences of the water/substrate and water/vacuum interfaces on the results reported here. Therefore, future experiments that can explore these processes in thicker films are needed to test this conjecture.

The structural changes in the D_2O film vs the number of heat pulses, N_p, were investigated using reflection absorption infrared spectroscopy (RAIRS). The spectra were collected while the sample was kinetically arrested at 70 K and are sensitive to the hydrogen-bonding configuration of the molecules, thereby providing information about their structural arrangement within the film.[43–46] By collecting all spectra at 70 K, independent of T_{max}, we avoid thermal effects that can lead to artificial isosbestic points.[47,48] Additionally, the kinetically arrested films provide IR spectra related to the inherent structures measured by MD simulations.[1,2,49] While the IR spectra are sensitive to the local structure, they are complementary to more direct measurements of the structure, such as those obtained by diffraction techniques.[50–53] Furthermore, because of the complicated effects of isotopic substitution on the IR spectra,[43,54] we cannot make direct comparisons of the structures of D_2O and H_2O. Instead, as we show below, the IR spectra allow us to track structural changes in D_2O vs time and temperature. We compare these changes to similar measurements on H_2O to compare the isotope effects in supercooled water. Finally, we observe that prior to crystallization, the IR spectra can always be decomposed into two components. We hypothesize that these two components are related to the HDL-like and LDL-like structural motifs that are postulated to exist in water.[1,2] However, we do not measure the density, or density changes, in the water films in the current experiments.

For the pulsed heating experiments, the ASW films were prepared in one of two initial configurations, which we refer to as hyper-quenched water (HQW) and low-density amorphous water (LDA).[13,14] HQW was prepared by transiently heating the nanoscale

film to ~300 K for three laser pulses, during which the sample was at or near the peak temperature, T_{max}, for ~3 ns/pulse. Figure S1 of the supplementary material shows $T(t)$ at the vacuum surface for a 50 ML thick water film. LDA was prepared by thermally annealing the sample near the glass transition temperature ($T_g \approx 136$ K[55]) for ≥130 s. Because the structure of our LDA films, as measured by infrared spectroscopy, does not change appreciably for isothermal annealing temperatures above 130 K, the precise annealing temperature used to form LDA is not critical (so long as crystallization is avoided). Any memory of the initial structure of the ASW film is lost in the preparation of the LDA or HQW states. For example, Fig. S2 demonstrates that an LDA film prepared by first heating the ASW film to 300 K to produce HQW before annealing at low temperatures has the same IR spectra as an ASW film that was directly annealed to produce LDA. Likewise, HQW is the same if produced directly from ASW or indirectly from LDA. We have also verified that the relaxation kinetics and steady-state structure at intermediate temperatures, which are described in Sec. III, are the same for either direct or "indirect" preparation of the starting configuration.

We assume LDA to be equivalent to quenched LDL as it is prepared by annealing at or near T_g. However, due to the finite cooling rate of the experiment and the rapid equilibration of mildly supercooled water, we do not expect HQW to have the same structure as the room temperature liquid. Instead, as described in Sec. III, HQW represents the (quenched) structure of D_2O at ~250 K.[13] Currently, we do not have a reliable method for measuring the spectra for quenched, room temperature water, or for determining it from the spectra of LDA and HQW. Furthermore, while water at ambient pressure and temperature is expected to be an inhomogeneous mixture with HDL-like and LDL-like structural motifs where the fraction of the HDL-like component increases with increasing temperature,[1,2] various definitions for the two structural components can lead to quite different predictions for their relative abundance as a function of temperature and pressure.[2,56–58] Therefore, while HQW is expected to be a mixture of both the HDL and LDL structural motifs, we do not know their relative abundance.

The HQW formed in our pulsed heating experiments is distinct from hyper-quenched glassy water, HGW, which is formed by the rapid quenching of micrometer-sized liquid droplets on a cryogenic substrate.[59,60] An important difference between the two techniques is the cooling rate, which is ~5×10^9 K/s for pulsed heating and ≤10^7 K/s for splat quenching. As a result of the lower cooling rate in the splat quenching process, the water remains at or near its equilibrium structure as it cools to cryogenic temperatures. With careful optimization, the cooling rates obtained by splat quenching are just high enough to avoid measurable crystallization in HGW,[59] while less than optimal conditions result in crystalline fractions of a few percent or more.[60] Because the time to crystallize is always longer than the structural relaxation time,[14] this suggests that HGW has sufficient time to equilibrate to the structure of LDA as it cools. The observation that the structures of LDA and HGW are the same also supports this hypothesis.[53]

III. RESULTS AND DISCUSSION

A. Absorption spectra

Figure 1(a) shows representative IR spectra of the OD stretching region for HQW and LDA, as well as crystalline ice (CI). HQW exhibits a maximum at ~2534 cm^{-1}, while LDA is red shifted with a maximum at 2524 cm^{-1} and increased intensity. CI, produced by transiently heating the film to T_{max} = 210 K for N_p = 9410, is further red shifted with a maximum at 2499 cm^{-1} and exhibits sharper spectral features than those of either HQW or LDA. The systematic changes in the IR spectra that occur upon transiently heating the D_2O film can be most readily seen in the difference spectra, which are formed by subtracting the LDA spectrum from all the subsequent spectra. Figure 1(b) demonstrates the evolution of the difference spectra for heating to an intermediate temperature, T_{max} = 215 K, when starting with LDA (LDA_i – blue curves) or HQW (HQW_i – red curves). The difference spectra emphasize the isosbestic points at ~2540 and ~2300 cm^{-1}, and the arrows in Fig. 1(b) indicate the direction of the changes to the positive, high frequency peak in the difference spectra (centered at ~2580 cm^{-1}) with increasing N_p. This peak grows when heating LDA_i and decreases when heating HQW_i toward approximately the same intermediate value prior to crystallization. When N_p = 505 (±5), the spectra

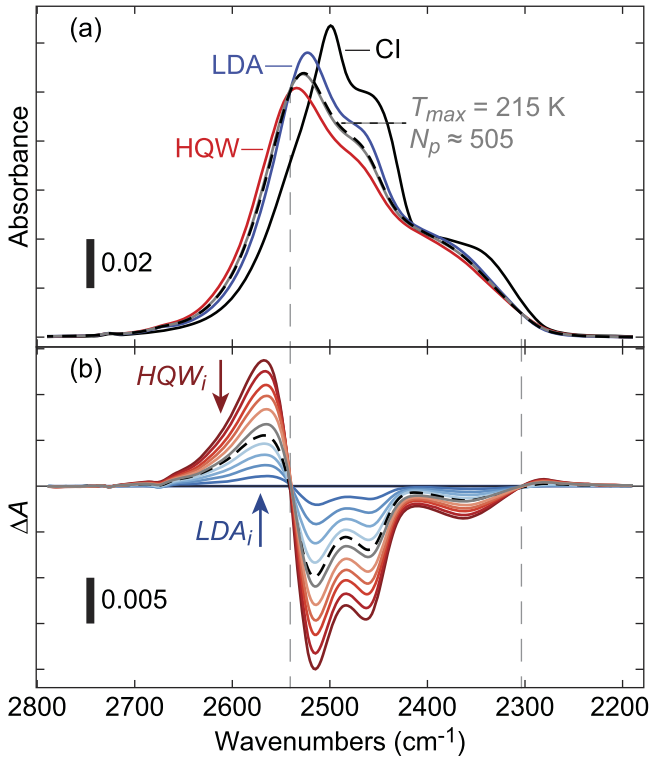

FIG. 1. Infrared absorption spectra of transiently heated D_2O films across the OD stretch region. (a) HQW (red), LDA (blue), and CI (solid black). CI was produced by heating at T_{max} = 210 K for N_p = 9410. Steady-state spectra obtained prior to crystallization at T_{max} = 215 K (N_p = 505 ± 5) starting from HQW_i (gray) and LDA_i (dashed black) are also shown. (b) Difference spectra, obtained by subtracting the LDA spectrum, for experiments with LDA_i (dark to light blue to dashed black) and HQW_i (dark to light red to gray) when heated to T_{max} = 215 K with arrows indicating the change with increasing N_p. The LDA_i spectra shown are from N_p = 0, 15, 45, 130, 260, and 510 and the HQW_i spectra are from N_p = 0, 1, 4, 10, 40, and 500. The gray dashed vertical lines in (a) and (b) show the location of two isosbestic points.

from both initial configurations are identical within the error of the experiment and are shown as the overlapping solid gray and dashed black spectra in Fig. 1(a). The corresponding difference spectra exhibit a small difference in ΔA due to slight variations in T_{max}; however, this difference is less than 2% of the absorbance spectrum.

For water in the OH-stretch band, stronger hydrogen bonds, such as molecules in a tetrahedral bonding geometry, are associated with lower vibrational frequencies, while weaker, often distorted bonds are typically at higher frequencies.[43,61–65] Thus, the spectrum for crystalline D_2O in Fig. 1(a) is red shifted relative to LDA and HQW, which are both non-crystalline. Previous research has shown that the Raman spectra for LDA are also red shifted compared to those for high density amorphous (HDA).[46,66–68] The differences between the spectra for LDA and HQW are reminiscent of those between LDA and HDA, however, because HQW is a mixture of LDA and HDA, the differences are less pronounced.

All of the IR spectra can be reproduced as a linear combination of the HQW, LDA, and CI spectra as demonstrated in Fig. S3 of the supplementary material. As a result, the fraction of each component, f_{HQW}, f_{LDA}, and f_{CI}, can, therefore, be determined as a function of N_p at a given T_{max}. For the remainder of this work, we will focus on f_{HQW} prior to appreciable crystallization (i.e., $f_{CI} < 0.02$).

B. Reversible structural changes and steady-state structure

In Fig. 2, f_{HQW} is shown as a function of N_p for three different intermediate temperatures when starting with HQW_i (red) and LDA_i (blue). At any temperature, f_{HQW} asymptotes toward a steady-state value, f^{SS}_{HQW}, that depends on T_{max} but is independent of the initial structural configuration. For the temperatures shown here, $f^{SS}_{HQW}(T_{\max}) \approx 0.23$, 0.45, and 0.78 at T_{max} = 205, 215, and 231 K, respectively. As was seen previously with H_2O, the structural changes are reversible,[13] meaning that upon changing T_{max}, f_{HQW} trends toward the new value of f^{SS}_{HQW} corresponding to that temperature as shown in Fig. 3.

The data shown in Fig. 3 were collected by preparing the sample into either initial configuration then heating to T_{max} = 221 K. Once the system had approached the structurally equilibrated steady-state liquid, the temperature was changed to drive it back toward the starting configuration of HQW or LDA by heating at T_{max} = 256 K or annealing at T_g, respectively. This process was repeated several times, and the first three temperature cycles are shown for HQW_i [Fig. 3(a)] and LDA_i [Fig. 3(b)]. For these experiments, the crystalline fraction within the film increases as N_p increases, but f_{CI} was still less than 0.02 after three temperature cycles (Fig. 3, gray diamonds). With HQW_i, $f_{CI} < 0.02$ even after five heating cycles, but due to the larger number of pulses needed to relax LDA_i, f_{CI} exceeded 0.02 after four cycles in that case (not shown). However, the liquid fraction of the D_2O sample continued to reversibly change between structural motifs even after the onset of crystallization. The spectral changes in Figs. 1 and 3 indicate that the observed structural changes are not due to irreversible transformations associated with crystallization,[69] crossing a spinodal,[70] or pore collapse.[71]

As mentioned already, f^{SS}_{HQW} does not depend on whether the experiments start from HQW_i or LDA_i. In addition, the steady-state structure does not depend on whether the nanoscale water films are

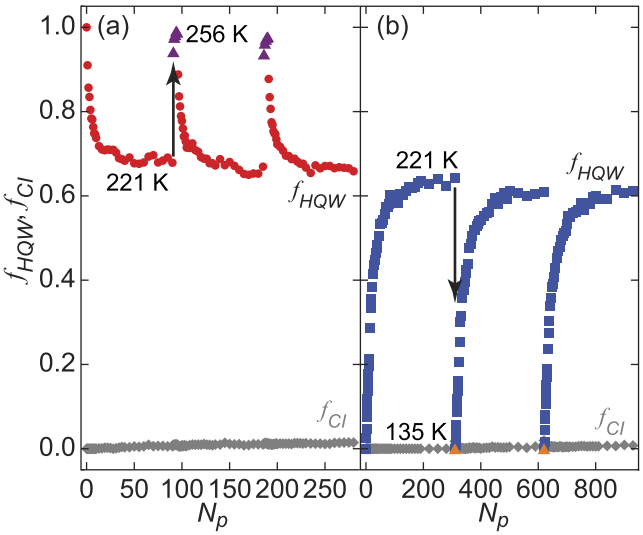

FIG. 3. Reversible structural changes for D_2O. (a) Starting from HQW_i, the sample was heated at T_{max} = 221 K for N_p = 90 (red circles), then heated at T_{max} = 256 K for N_p = 5 (purple triangles). This cycle was repeated three times. The fraction crystalline, f_{CI}, is shown as gray diamonds. (b) LDA_i heated at T_{max} = 221 K for N_p = 310 (blue squares), then annealed at T_g (135 K) for 130 s (orange triangle).

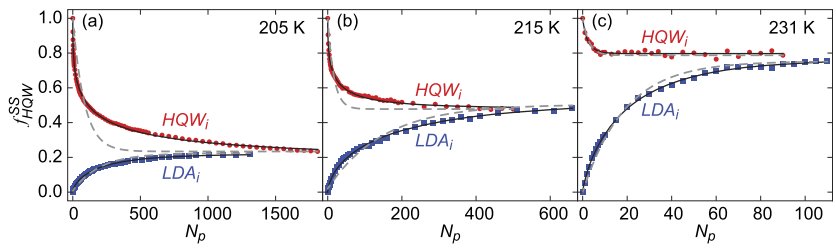

FIG. 2. Examples of f_{HQW} vs N_p for HQW_i (red circles) and LDA_i (blue squares) at three representative temperatures. (a) 205 K, $f^{SS}_{HQW} \approx 0.23$; (b) 215 K, $f^{SS}_{HQW} \approx 0.45$; and (c) 231 K, $f^{SS}_{HQW} \approx 0.78$. Stretched exponential fits are overlaid in black and simple exponential fits are shown as dashed gray curves. Data collected on the graphene/Pt(111) substrate except for HQW_i at 205 and 231 K, which were collected on the Pt(111) substrate.

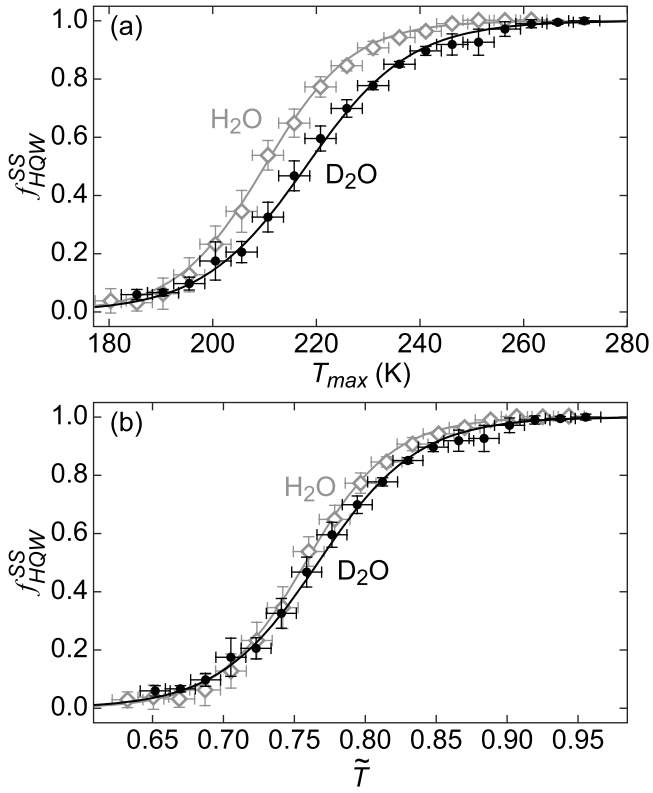

FIG. 4. Steady-state structural composition for D_2O (solid symbols) and H_2O[13] (open symbols). (a) Steady-state fraction, f^{SS}_{HQW}, vs T_{max}. The results are the average of experiments with HQW_i and LDA_i on both Pt(111) and graphene/Pt(111), and the vertical error bars show the standard deviation, while the horizontal error bars indicate the ±3 K uncertainty in T_{max}. The solid lines show logistic function fits to the data. (b) f^{SS}_{HQW} vs the reduced temperature $\tilde{T} = T_{max}/T_{MD}$.

adsorbed on Pt(111) or graphene/Pt(111). Therefore, we can calculate f^{SS}_{HQW} vs T_{max} from the average of individual experiments with both initial configurations on both substrates [see Fig. 4(a), black circles]. At temperatures below ~190 K, the LDA structural motif is dominant ($f^{SS}_{HQW} \approx 0$). Since the measurements are related to the inherent structures that can be calculated in MD simulations,[1,2,49] the results show that the inherent structure for D_2O at low temperatures is essentially obtained already at ~190 K. Above ~190 K, the fraction of HQW increases and is the dominant motif above ~250 K. The data can be fit by a logistic function,[4] $f^{SS}_{HQW}(T_{\max}) = (1 + \exp[-(T_{max} - T_0)/\Delta T])^{-1}$, with T_0 = 218 K and ΔT = 10 K [see Fig. 4(a), black line].[72] For T_{max} > 255 K, f^{SS}_{HQW} is ~1 due to the rapid structural equilibration of mildly supercooled heavy water and the experiment's finite cooling rate, which results in the loss of structural information at high temperatures.[13] Thus, the structure of HQW, prepared by heating to ~300 K, should reflect the (quenched) structure of D_2O somewhat below ~255 K. While we cannot unambiguously determine the composition of HQW, the temperature range where the experiments are sensitive to the structure, below 255 K, overlaps with the temperatures where previous x-ray scattering measurements began to observe rapid structural changes.[8,28]

In Fig. 4(a), the gray diamonds and gray line show the previously determined f^{SS}_{HQW} values for H_2O and the corresponding fit with the logistic function (T_0 = 210 K and ΔT = 8.5 K).[13] The results show that the temperature range over which the structure changes from predominantly HQW to LDA occurs at a lower temperature for H_2O than D_2O. Previous experiments show that D_2O has a more tetrahedrally ordered structure than H_2O at a given temperature.[8,20–30,73–75] Because the current experiments show that the fraction LDA is larger (i.e., f^{SS}_{HQW} is smaller) for D_2O than H_2O at any given temperature, and recalling that LDA corresponds to more nearly tetrahedral bonding, the results show that the previously reported structural differences between the isotopologues also extend to much lower temperatures.

As discussed in the introduction, Limmer and Chandler proposed that the temperature of maximum density, T_{MD}, provides a convenient, isostructural point for the comparison of different water models in classical MD simulations.[33] Applying their suggestion to D_2O and H_2O, Fig. 4(b) shows the structural changes as a function of the reduced temperature, $\tilde{T} = T_{max}/T_{MD}$,[33] where T_{MD} = 277.13 K for H_2O and 284.34 K for D_2O.[18] Upon scaling the temperatures, the data for the isotopologues collapse onto each other, within error, supporting the idea that T_{MD} provides an isostructural point for comparison of liquid and supercooled water.

If there is a liquid–liquid critical point for water, then the Widom line is the extension (in pressure and temperature) of the coexistence line into the supercritical region. Along an isobar, the Widom line corresponds to the point where the structure of the liquid is changing the most rapidly with temperature. Experiments on supercooled water droplets placed the Widom line at 233 and 229 K for D_2O and H_2O, respectively.[8] For the current experiments, the structure is apparently changing the most rapidly at ~218 K for D_2O [see Fig. 4(a)]. However, this difference is due to limitations of the pulsed heating technique and does not necessarily indicate a discrepancy with the earlier measurements. In particular, because our experiments are not sensitive to the changes in the structure of water for temperatures above ~250 K, our experiments underestimate the width of the transition from the high to low temperature structures.[13] However, because of the ability of the pulsed heating technique to follow the structural changes improves at lower temperatures, it should accurately reflect the low temperature threshold (i.e., at ~190 K).

C. Structural relaxation

While f^{SS}_{HQW} is independent of the initial configuration, Fig. 2 shows that the rate at which supercooled D_2O relaxes to its steady-state structure depends on the initial configuration. At temperatures above ~240 K, the relaxation can be well fit by a simple exponential function for both HQW_i and LDA_i (data not shown). However, as the temperature decreases below 240 K, the relaxation can no longer be described by simple exponential kinetics. Instead, a stretched exponential of the general form $f_{HQW} = \exp[-(N_p/N^*)^{\beta}]$ provides a more accurate fit to the data, as shown by the black lines in Figs. 2 and S4. Here, β is the stretching parameter and N^* is a constant that is related to the average number of pulses needed to relax the structure, N_{rel}, where $N_{rel} = N^*\beta^{-1}\Gamma(\beta^{-1})$.[76] For a stretched exponential, β

is less than 1, and smaller values of β correspond to larger deviations from simple exponential relaxation. For comparison, the dashed gray lines in Fig. 2 (and Fig. S4) indicate the simple exponential fits.

The values of N_{rel} and β, determined from the fits to the relaxation vs N_p for each T_{max}, are shown in Fig. 5 for both HQW_i (red circles) and LDA_i (blue squares). As expected, the time required for D_2O to relax, which is proportional to N_{rel}, increases rapidly as the temperature decreases [Fig. 5(a)]. N_{rel} spans a range from ~7000 pulses at 185 K for HQW_i, to ~1 pulse for LDA_i at 266 K. In our previous study on H_2O, we used a simple approximation to relate N_{rel} to data obtained by other techniques, where we assume that the structural relaxation occurs during some time window, δt_{pulse}, when the temperature is near T_{max}, and therefore, the relaxation time is roughly $\tau_{rel} \sim \delta t_{pulse} N_{rel}$.[14] Using δt_{pulse} = 1 ns, as was done previously,[14] τ_{rel} spans a range from ~7 × 10^{-6} s for HQW_i at 185 K to ~1 × 10^{-9} s at 266 K for LDA_i [see Fig. 5(a), right axis] Note that the relaxation measured here is the molecular rearrangement for D_2O from an initial metastable equilibrium configuration toward a new metastable equilibrium configuration in response to a temperature change. This non-equilibrium relaxation process, which is similar to aging experiments in glasses as they approach equilibrium,[14,77–80] is distinct from equilibrium structural relaxation measurements that involve monitoring the response to small perturbations.[18,25,30] For aging in glasses, it is often found that the structural relaxation rate at a given temperature depends on whether the temperature jump was positive or negative,[77,81–83] which is similar to the behavior seen here for supercooled D_2O (Figs. 2 and 5).

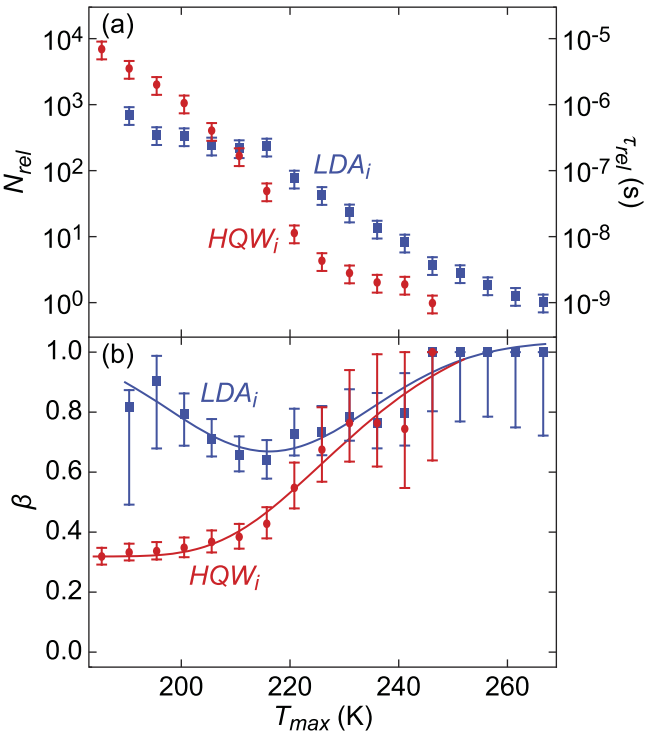

FIG. 5. The relaxation rate of D_2O as a function of T_{max}. (a) The effective number of pulses to relax the sample, N_{rel}, for HQW_i (red circles) and LDA_i (blue squares). The error bars are estimated to be 30% of the value of N_{rel}. The right-hand side shows the approximate relaxation time, τ_{rel}. (b) The stretching parameter, β, determined from the stretched exponential fits of $f_{HQW}(N_p)$ for HQW_i (red circles) and LDA_i (blue squares). The error bars were determined from a 1% deviation of the target function.[14] Curves are provided as a guide for the eye.

Figure 5(b) shows the stretching parameter, β, as a function of T_{max} when starting from HQW_i (red circles) and LDA_i (blue squares). As the temperature is decreased, β initially decreases for both LDA_i and HQW_i. At T_{max} = 215 K, the value of β for LDA_i reaches a minimum and increases upon further cooling, while the value of β for HQW_i levels off at $\beta \approx 0.4$ at low temperatures. For $T_{max} \geq 240$ K, the relaxation rates are sufficiently fast that it is difficult to determine the values for β, which leads to the large uncertainty shown in Fig. 5(b) for both starting configurations. However, we expect that the kinetics in this temperature range can be described by a simple exponential relaxation ($\beta = 1$). For LDA_i, N_{rel} vs temperature has a notable change in slope at ~215 K, which is at the same temperature where β reaches a minimum. As discussed below, this behavior is also found in H_2O at the same reduced temperature (see Fig. 6). However, because these experiments involve relaxation toward steady state, as opposed to relaxation at or near equilibrium, it is challenging to relate them to possible equilibrium processes that have been discussed in the literature, such as a fragile-to-strong transition[2,84] or a "dynamic Schottky band."[85]

D. Structural and dynamical heterogeneities in supercooled water

Stretched exponential kinetics are frequently observed in glasses and supercooled liquids and are often attributed to dynamical heterogeneities, which likely arise due to spatial heterogeneities within the liquid.[80,86] Qualitatively, these spatial heterogeneities are associated with regions in which particles are "jammed," thus experiencing slower relaxation, and regions where the particles are able to move more freely and have faster relaxation. Smaller values of β typically indicate greater spatial heterogeneities within the film. However, it is important to note that these dynamical heterogeneities are distinct from the structural heterogeneities associated with the HDL and LDL structural motifs in water. In particular, "normal" liquids, which do not have these structural heterogeneities, can still exhibit the dynamical, spatial heterogeneities described above.

The relation between dynamical and structural heterogeneities in supercooled water is still a matter of discussion.[85,87] However, comparing the relaxation kinetics for supercooled D_2O and H_2O in the region where the steady-state structures are changing rapidly as a function of temperature provides an opportunity to explore the connections between the structural and dynamical heterogeneities. Figures 6(a) and 6(b) show N_{rel} and β vs $\tilde{T}$ for both D_2O and H_2O. When scaled by the isostructural point, the relaxation rates and stretching parameters for the isotopologues agree remarkably well for both HQW_i and LDA_i. For comparison, the relaxation rates as a function of T_{max} are shown in Fig. S5. The observation that T_{MD} scaling works well for the steady-state structure [see Fig. 4(b)] and the relaxation kinetics [Figs. 6(a) and 6(b)] suggests a close link between the structural heterogeneities in water and the kinetics. The complete relaxation traces for several individual experiments, compared

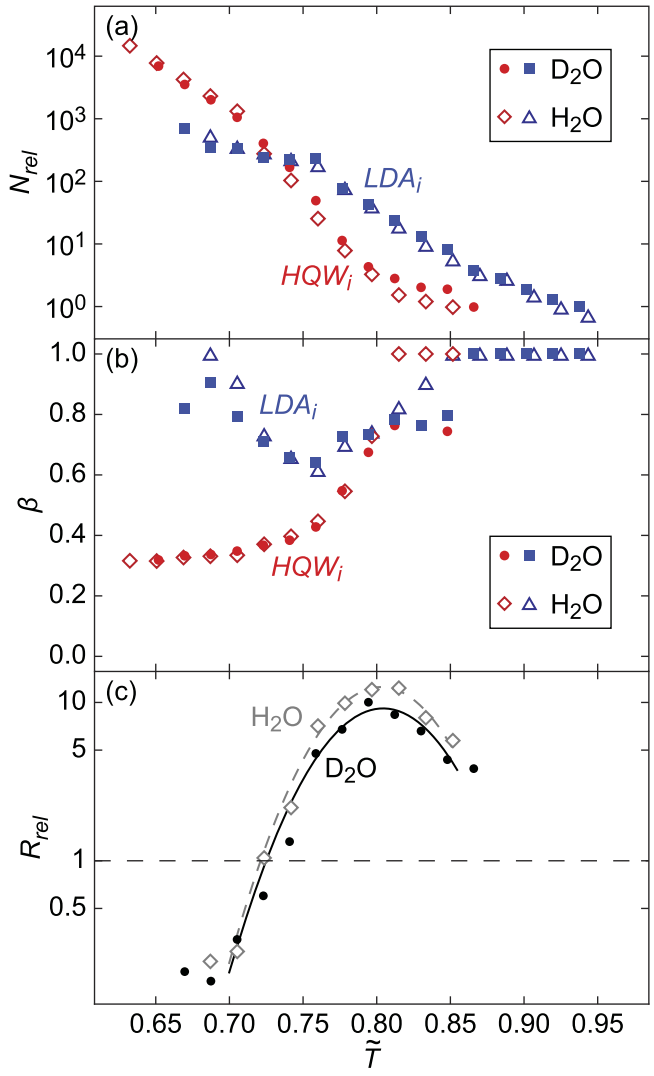

FIG. 6. Relaxation kinetics for D_2O (solid symbols) and H_2O[14] (open symbols). (a) N_{rel} vs $\tilde{T}$ for HQW_i (red) and LDA_i (blue), on graphene/Pt(111). (b) β vs $\tilde{T}$ for HQW_i (red) and LDA_i (blue). (c) $R_{rel} = N_{rel}^{LDA_i}/N_{rel}^{HQW_i}$, with curves to guide the eye. A dashed line at $R_{rel} = 1$ indicates where LDA_i and HQW_i relax at the same rate. D_2O is shown as black circles and H_2O as gray open diamonds.

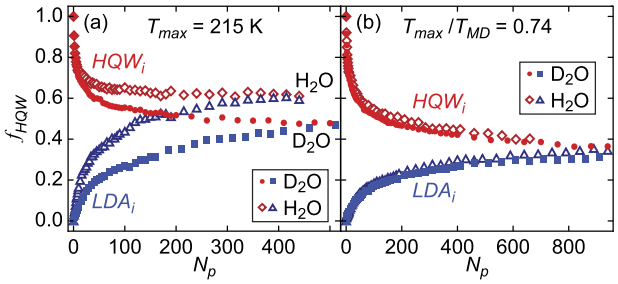

FIG. 7. Comparison of the structural relaxation for D_2O (solid symbols) and H_2O (open symbols), for HQW_i (red) and LDA_i (blue). (a) Comparison of the isotopologues at the same temperature, T_{max} = 215 K, where f_{HQW}^{SS} (D_2O) = 0.47 and f_{HQW}^{SS} (H_2O) = 0.65. (b) Comparison at the same reduced temperature, $\tilde{T}$ = 0.74, where $f_{HQW}^{SS} = 0.34 \pm 0.05$ for both isotopologues. The D_2O data in panel (b) were collected at T_{max} = 210 K and H_2O at T_{max} = 205 K.

at the same T_{max} or the same reduced temperature, are shown in Fig. 7. The similarity of the kinetics at the same $\tilde{T}$ [Fig. 7(b)] also supports the connection between the structural heterogeneities and the kinetics.

When comparing the relaxation of the two different initial configurations of a given isotopologue, it is instructive to examine the ratio of effective relaxation, R_{rel}, as shown in Fig. 6(c), where $R_{rel} = N_{rel}^{LDA_i}/N_{rel}^{HQW_i}$. At high temperatures, relaxation is faster from HQW_i than LDA_i with a maximum in R_{rel} at $\tilde{T} \approx 0.8$, where HQW_i relaxes ~10 times faster than LDA_i. As $\tilde{T}$ is decreased, the relaxation ratio also decreases and reaches $R_{rel} = 1$ at $\tilde{T} \approx 0.73$, where the two initial configurations relax at approximately the same rate. Upon further cooling, LDA_i relaxes faster for both D_2O and H_2O. From the perspective of the potential energy landscape for supercooled water, the trends in R_{rel} suggest that the relaxation is the fastest for the initial configuration that starts the "closest" to the final configuration of interest. In this picture, LDA_i ($HQWi$) relaxes more quickly at lower (higher) final temperatures because the structure there is still predominantly LDA (HQW), and thus, fewer changes are required. Alternatively, it has been proposed that LDL is a strong liquid, while HDL is a fragile liquid.[84,88] In that scenario, because fragile liquids slow down dramatically as they cool, the stronger temperature dependence for $N_{rel}^{HQW_i}$ compared to $N_{rel}^{LDA_i}$ [see Figs. 5(a) and 6(a)] could be explained by HQW having a larger fraction of HDL compared to LDA.

The results shown in Figs. 6 and 7 suggest that most of the differences in the kinetics for D_2O and H_2O at any given temperature are related to the fact that the steady-state structures are different. However, when considering kinetic isotope effects (KIE), one typically compares the rates of reaction for the isotopologues at the same temperature assuming that the systems are otherwise essentially the same. Because the ensemble of barriers that govern relaxation are different for D_2O and H_2O at any given temperature, the ratio of the relaxation rates exhibits large variations vs T_{max} (not shown). On the other hand, comparing the rates at the same $\tilde{T}$ is also problematic because the actual temperatures are different. Ideally, to estimate the KIE for water, one would compare the relaxation rates for H_2O and D_2O when they have both the same structure (i.e., the same ensemble of barriers) and the same temperature. An approach for estimating this based on a simple model for the relaxation kinetics for H_2O[14] is described in the supplementary material (see Estimate of the Kinetic Isotope Effect in Supercooled Water). Within the uncertainties, the results suggest that H_2O relaxes ~1–2 times faster for 180 K < T_{max} < 245 K (see Fig. S6).

While the agreement between H_2O and D_2O with the T_{MD} scaling is quite good, we have also analyzed the data using the thermal offset conjecture. With an effective offset equal to the difference in T_{MD}, as was originally proposed by Vedamuthu *et al.*,[22] the isotopologues also exhibit good agreement for both f_{HQW}^{SS} and N_{rel} as shown in Fig. 8. Therefore, from these data alone, there is no compelling

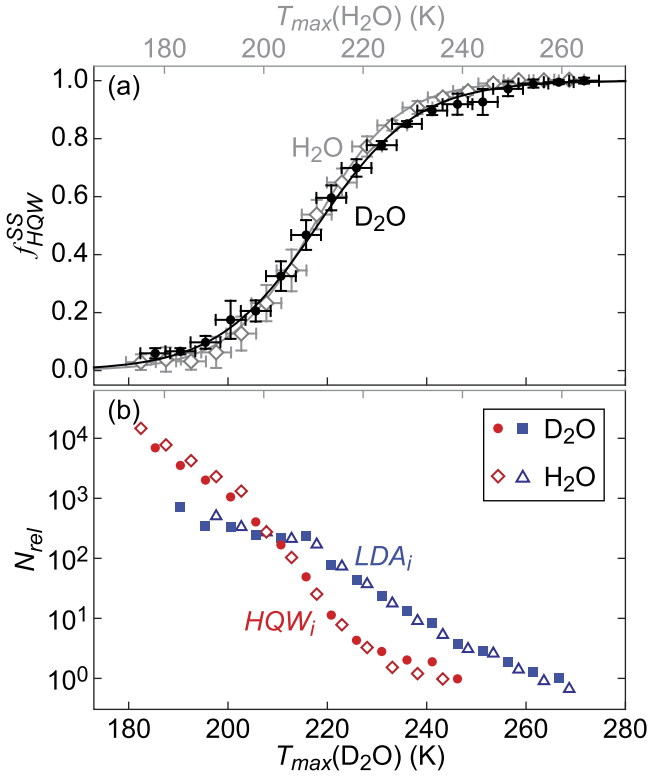

FIG. 8. The stretched exponential fit parameters for D_2O (solid symbols) and H_2O[13,14] (open symbols) when an effective thermal offset of 7.2 K has been applied to the H_2O values.[22] (a) f^{SS}_{HQW} with error bars given by the standard deviation with the logistic fits is overlaid. (b) N_{rel} for HQW_i (red) and LDA_i (blue).

argument for one approach over the other as both models work equally well. However, the thermal offset is typically used as a fitting parameter to reproduce various properties,[8,24,26–29] which removes any physical basis for the approach. Therefore, we believe the corresponding states argument of Limmer and Chandler,[33] originally designed to examine the dynamics of several classical water models, is a more attractive approach to examine the isotope effects of water. The approach is quantitatively similar to the thermal offset conjecture while also providing a reasonable physical explanation for the results.

Although the focus of this work has been on the H/D isotope effects, it is important to note that the $^{16}O/^{18}O$ isotope effects are expected to be dominated by classical mass effects rather than the NQEs, which dominate the H/D isotope effects.[18] Therefore, while D_2O and $H_2{}^{18}O$ have the same molecular mass, the isotope effects on the heavy oxygen water are expected to be smaller, with dynamic behavior closer to that of H_2O.[29,30] Preliminary results of $H_2{}^{18}O$ starting from LDA_i at temperatures above 240 K indicate that, as expected, it relaxes at a rate more similar to H_2O than D_2O, see Fig. S7. The difference between the relaxation of D_2O and $H_2{}^{18}O$ further highlights the quantum effects resulting upon H/D substitution.

IV. CONCLUSIONS

We have examined the structural relaxation of nanoscale D_2O films from 185 K to 255 K, greatly extending the temperature range over which structural information is available. D_2O exhibits a temperature dependent transition between two structural motifs, which can be described by a logistic function centered at 218 K. For temperatures below 185 K, D_2O's structure has converged to that obtained by annealing at the glass transition temperature. The structural relaxation exhibited stretched exponential kinetics, suggestive of dynamic heterogeneity within the sample, and relaxation rates that depend on the initial structural configuration. At a given temperature, the D_2O films have slower relaxation rates than H_2O and have more tetrahedral, ice-like character. However, using reduced temperatures $\tilde{T} = T_{max}/T_{MD}$, the structural transition and effective relaxation of the isotopologues show a common response. These results are consistent with the corresponding states principle demonstrated by Chandler and Limmer[33] for the dynamics of several classical water models. This approach is quantitatively similar to the thermal offset conjecture that is often used to compare the temperature-dependent properties of H_2O and D_2O but is attractive since it provides a reasonable physical explanation for the results.

SUPPLEMENTARY MATERIAL

The supplementary material provides additional information on the linear combination fits of the absorption spectra, stretched exponential relaxation, kinetic isotope effects, and comparison with $H_2{}^{18}O$ structural relaxation (Figs. S1–S7).

ACKNOWLEDGMENTS

This work was supported by the U.S. Department of Energy (DOE), Office of Science, Office of Basic Energy Sciences, Division of Chemical Sciences, Geosciences, and Biosciences. This research study was performed in EMSL, a national scientific user facility sponsored by DOE's Office of Biological and Environmental Research and located at the Pacific Northwest National Laboratory, which is operated by Battelle for DOE.

AUTHOR DECLARATIONS

Conflict of Interest

The authors declare no conflicts of interest.

Author Contributions

The research was designed and supervised by G.A.K. and B.D.K. L.K. and W.A.T. conducted the experiments and analyzed the data. L.K. wrote the manuscript, with input from all authors.

DATA AVAILABILITY

The data that support the findings of this study are available within the article and its supplementary material or are available from the corresponding author upon reasonable request.

REFERENCES

[1] A. Nilsson and L. G. M. Pettersson, Nat. Commun. **6**, 8998 (2015).
[2] P. Gallo, K. Amann-Winkel, C. A. Angell, M. A. Anisimov, F. Caupin, C. Chakravarty, E. Lascaris, T. Loerting, A. Z. Panagiotopoulos, J. Russo, J. A. Sellberg, H. E. Stanley, H. Tanaka, C. Vega, L. Xu, and L. G. M. Pettersson, Chem. Rev. **116**, 7463–7500 (2016).
[3] J. C. Palmer, P. H. Poole, F. Sciortino, and P. G. Debenedetti, Chem. Rev. **118**, 9129–9151 (2018).
[4] N. J. Hestand and J. L. Skinner, J. Chem. Phys. **149**, 140901 (2018).
[5] R. Shi and H. Tanaka, Proc. Natl. Acad. Sci. U. S. A. **117**, 26591–26599 (2020).
[6] O. Mishima and H. E. Stanley, Nature **396**, 329–335 (1998).
[7] J. A. Sellberg, C. Huang, T. A. McQueen, N. D. Loh, H. Laksmono, D. Schlesinger, R. G. Sierra, D. Nordlund, C. Y. Hampton, D. Starodub, D. P. DePonte, M. Beye, C. Chen, A. V. Martin, A. Barty, K. T. Wikfeldt, T. M. Weiss, C. Caronna, J. Feldkamp, L. B. Skinner, M. M. Seibert, M. Messerschmidt, G. J. Williams, S. Boutet, L. G. M. Pettersson, M. J. Bogan, and A. Nilsson, Nature **510**, 381–384 (2014).
[8] K. H. Kim, A. Späh, H. Pathak, F. Perakis, D. Mariedahl, K. Amann-Winkel, J. A. Sellberg, J. H. Lee, S. Kim, J. Park, K. H. Nam, T. Katayama, and A. Nilsson, Science **358**, 1589–1593 (2017).
[9] S. Cerveny, F. Mallamace, J. Swenson, M. Vogel, and L. Xu, Chem. Rev. **116**, 7608–7625 (2016).
[10] K. H. Kim, K. Amann-Winkel, N. Giovambattista, A. Späh, F. Perakis, H. Pathak, M. L. Parada, C. Yang, D. Mariedahl, T. Eklund, T. J. Lane, S. You, S. Jeong, M. Weston, J. H. Lee, I. Eom, M. Kim, J. Park, S. H. Chun, P. H. Poole, and A. Nilsson, Science **370**, 978–982 (2020).
[11] Y. Xu, C. J. Dibble, N. G. Petrik, R. S. Smith, A. G. Joly, R. G. Tonkyn, B. D. Kay, and G. A. Kimmel, J. Chem. Phys. **144**, 164201 (2016).
[12] Y. Xu, N. G. Petrik, R. S. Smith, B. D. Kay, and G. A. Kimmel, Proc. Natl. Acad. Sci. U. S. A. **113**, 14921–14925 (2016).
[13] L. Kringle, W. A. Thornley, B. D. Kay, and G. A. Kimmel, Science **369**, 1490–1492 (2020).
[14] L. Kringle, W. A. Thornley, B. D. Kay, and G. A. Kimmel, Proc. Natl. Acad. Sci. U. S. A. **118**, e2022884118 (2021).
[15] M. Holz, X. A. Mao, D. Seiferling, and A. Sacco, J. Chem. Phys. **104**, 669–679 (1996).
[16] E. H. Hardy, A. Zygar, M. D. Zeidler, M. Holz, and F. D. Sacher, J. Chem. Phys. **114**, 3174–3181 (2001).
[17] H. W. Xiang, *The Corresponding-States Principle and Its Practice; Thermodynamic, Transport and Surface Properties of Fluids* (Elsevier B.V., Amsterdam, 2005).
[18] M. Ceriotti, W. Fang, P. G. Kusalik, R. H. McKenzie, A. Michaelides, M. A. Morales, and T. E. Markland, Chem. Rev. **116**, 7529–7550 (2016).
[19] S. Habershon, T. E. Markland, and D. E. Manolopoulos, J. Chem. Phys. **131**, 024501 (2009).
[20] A. Eltareb, G. E. Lopez, and N. Giovambattista, Phys. Chem. Chem. Phys. **23**, 6914–6928 (2021).
[21] J. H. Root, P. A. Egelstaff, and A. Hime, Chem. Phys. **109**, 437–453 (1986).
[22] M. Vedamuthu, S. Singh, and G. W. Robinson, J. Phys. Chem. **100**, 3825–3827 (1996).
[23] F. X. Prielmeier, E. W. Lang, R. J. Speedy, and H.-D. Lüdemann, Ber. Bunsengesellschaft Phys. Chem. **92**, 1111–1117 (1988).
[24] C. H. Cho, J. Urquidi, S. Singh, and G. W. Robinson, J. Phys. Chem. B **103**, 1991–1994 (1999).
[25] C. Rønne, P.-O. Åstrand, and S. R. Keiding, Phys. Rev. Lett. **82**, 2888–2891 (1999).
[26] K. R. Harris, Phys. Chem. Chem. Phys. **4**, 5841–5845 (2002).
[27] K. R. Harris and L. A. Woolf, J. Chem. Eng. Data **49**, 1064–1069 (2004).
[28] K. H. Kim, H. Pathak, A. Spah, F. Perakis, D. Mariedahl, J. A. Sellberg, T. Katayama, Y. Harada, H. Ogasawara, L. G. M. Pettersson, and A. Nilsson, Phys. Rev. Lett. **119**, 075502 (2017).
[29] A. Berger, G. Ciardi, D. Sidler, P. Hamm, and A. Shalit, Proc. Natl. Acad. Sci. U. S. A. **116**, 2458–2463 (2019).
[30] B. Kutus, A. Shalit, P. Hamm, and J. Hunger, Phys. Chem. Chem. Phys. **23**, 5467–5473 (2021).
[31] C. Gainaru, A. L. Agapov, V. Fuentes-Landete, K. Amann-Winkel, H. Nelson, K. W. Köster, A. I. Kolesnikov, V. N. Novikov, R. Richert, R. Böhmer, T. Loerting, and A. P. Sokolov, Proc. Natl. Acad. Sci. U. S. A. **111**, 17402–17407 (2014).
[32] V. Fuentes-Landete, L. J. Plaga, M. Keppler, R. Bohmer, and T. Loerting, Phys. Rev. X **9**, 011015 (2019).
[33] D. T. Limmer and D. Chandler, Faraday Discuss. **167**, 485–498 (2013).
[34] G. A. Kimmel, K. P. Stevenson, Z. Dohnálek, R. S. Smith, and B. D. Kay, J. Chem. Phys. **114**, 5284–5294 (2001).
[35] K. P. Stevenson, G. A. Kimmel, Z. Dohnálek, R. S. Smith, and B. D. Kay, Science **283**, 1505–1507 (1999).
[36] T. Zubkov, R. S. Smith, T. R. Engstrom, and B. D. Kay, J. Chem. Phys. **127**, 184707 (2007).
[37] D. M. Murphy and T. Koop, Q. J. R. Meteorol. Soc. **131**, 1539–1565 (2005).
[38] W. Wagner, T. Riethmann, R. Feistel, and A. H. Harvey, J. Phys. Chem. Ref. Data **40**, 043103 (2011).
[39] Y. Xu, N. G. Petrik, R. S. Smith, B. D. Kay, and G. A. Kimmel, J. Phys. Chem. Lett. **8**, 5736–5743 (2017).
[40] L. Cheng, P. Fenter, K. L. Nagy, M. L. Schlegel, and N. C. Sturchio, Phys. Rev. Lett. **87**, 156103 (2001).
[41] G. Cicero, J. C. Grossman, E. Schwegler, F. Gygi, and G. Galli, J. Am. Chem. Soc. **130**, 1871–1878 (2008).
[42] D. C. Malaspina, E. P. Schulz, L. M. Alarcón, M. A. Frechero, and G. A. Appignanesi, Eur. Phys. J. E **32**, 35–42 (2010).
[43] B. M. Auer and J. L. Skinner, J. Chem. Phys. **128**, 224511 (2008).
[44] H. J. Bakker and J. L. Skinner, Chem. Rev. **110**, 1498–1517 (2010).
[45] Y. Ni and J. L. Skinner, J. Chem. Phys. **145**, 124509 (2016).
[46] C. J. Tainter, L. Shi, and J. L. Skinner, J. Chem. Phys. **140**, 134503 (2014).
[47] P. L. Geissler, J. Am. Chem. Soc. **127**, 14930–14935 (2005).
[48] J. D. Smith, C. D. Cappa, K. R. Wilson, R. C. Cohen, P. L. Geissler, and R. J. Saykally, Proc. Natl. Acad. Sci. U. S. A. **102**, 14171–14174 (2005).
[49] K. T. Wikfeldt, A. Nilsson, and L. G. M. Pettersson, Phys. Chem. Chem. Phys. **13**, 19918–19924 (2011).
[50] C. Benmore, L. C. Gallington, and E. Soignard, Mol. Phys. **117**, 2470–2476 (2019).
[51] L. B. Skinner, C. J. Benmore, J. C. Neuefeind, and J. B. Parise, J. Chem. Phys. **141**, 214507 (2014).
[52] C. Lin, J. S. Smith, S. V. Sinogeikin, and G. Shen, Proc. Natl. Acad. Sci. U. S. A. **115**, 2010–2015 (2018).
[53] D. T. Bowron, J. L. Finney, A. Hallbrucker, I. Kohl, T. Loerting, E. Mayer, and A. K. Soper, J. Chem. Phys. **125**, 194502 (2006).
[54] F. Li and J. L. Skinner, J. Chem. Phys. **133**, 244504 (2010).
[55] A. Hallbrucker, E. Mayer, and G. P. Johari, J. Phys. Chem. **93**, 4986–4990 (1989).
[56] P. H. Poole, F. Sciortino, U. Essmann, and H. E. Stanley, Nature **360**, 324–328 (1992).
[57] H. Tanaka, J. Chem. Phys. **112**, 799–809 (2000).
[58] V. Holten and M. A. Anisimov, Sci. Rep. **2**, 713 (2012).
[59] I. Kohl, L. Bachmann, A. Hallbrucker, E. Mayer, and T. Loerting, Phys. Chem. Chem. Phys. **7**, 3210–3220 (2005).
[60] E. Mayer, J. Appl. Phys. **58**, 663–667 (1985).
[61] Q. Sun, Vib. Spectrosc. **51**, 213–217 (2009).
[62] M. Yang and J. L. Skinner, Phys. Chem. Chem. Phys. **12**, 982–991 (2010).
[63] J. G. Davis, K. P. Gierszal, P. Wang, and D. Ben-Amotz, Nature **491**, 582–585 (2012).
[64] Q. Sun, Chem. Phys. Lett. **568–569**, 90–94 (2013).
[65] T. Morawietz, O. Marsalek, S. R. Pattenaude, L. M. Streacker, D. Ben-Amotz, and T. E. Markland, J. Phys. Chem. Lett. **9**, 851–857 (2018).
[66] D. D. Klug, O. Mishima, and E. Whalley, J. Chem. Phys. **86**, 5323–5328 (1987).
[67] H. Kanno, K. Tomikawa, and O. Mishima, Chem. Phys. Lett. **293**, 412–416 (1998).
[68] T. Loerting, C. Salzmann, I. Kohl, E. Mayer, and A. Hallbrucker, Phys. Chem. Chem. Phys. **3**, 5355–5357 (2001).
[69] D. T. Limmer and D. Chandler, J. Chem. Phys. **135**, 134503 (2011).

[70]R. J. Speedy, J. Phys. Chem. **86**, 982–991 (1982).
[71]C. R. Hill, C. Mitterdorfer, T. G. A. Youngs, D. T. Bowron, H. J. Fraser, and T. Loerting, Phys. Rev. Lett. **116**, 215501 (2016).
[72]Here, the logistic function is simply used to fit the data and other "switching" functions, such as the error function, will provide essentially identical information. The key properties are the mid-point and the width of the distribution.
[73]R. T. Hart, C. J. Benmore, J. Neuefeind, S. Kohara, B. Tomberli, and P. A. Egelstaff, Phys. Rev. Lett. **94**, 047801 (2005).
[74]A. K. Soper and C. J. Benmore, Phys. Rev. Lett. **101**, 065502 (2008).
[75]B. Tomberli, C. J. Benmore, P. A. Egelstaff, J. Neuefeind, and V. Honkimäki, J. Phys.: Condens. Matter **12**, 2597–2612 (2000).
[76]C. P. Lindsey and G. D. Patterson, J. Chem. Phys. **73**, 3348–3357 (1980).
[77]N. Giovambattista, H. E. Stanley, and F. Sciortino, Phys. Rev. E **69**, 050201 (2004).
[78]W. Kob, F. Sciortino, and P. Tartaglia, Europhys. Lett. **49**, 590–596 (2000).
[79]V. Lubchenko and P. G. Wolynes, J. Chem. Phys. **121**, 2852–2865 (2004).
[80]M. D. Ediger, C. A. Angell, and S. R. Nagel, J. Phys. Chem. **100**, 13200–13212 (1996).
[81]G. B. McKenna and S. L. Simon, Macromolecules **50**, 6333–6361 (2017).
[82]M. Lulli, C. S. Lee, H. Y. Deng, C. T. Yip, and C. H. Lam, Phys. Rev. Lett. **124**, 095501 (2020).
[83]C. A. Angell, K. L. Ngai, G. B. McKenna, P. F. McMillan, and S. W. Martin, J. Appl. Phys. **88**, 3113–3157 (2000).
[84]L. Xu, P. Kumar, S. V. Buldyrev, S.-H. Chen, P. H. Poole, F. Sciortino, and H. E. Stanley, Proc. Natl. Acad. Sci. U. S. A. **102**, 16558–16562 (2005).
[85]R. Shi, J. Russo, and H. Tanaka, Proc. Natl. Acad. Sci. U. S. A. **115**, 9444–9449 (2018).
[86]M. D. Ediger, Annu. Rev. Phys. Chem. **51**, 99–128 (2000).
[87]H. E. Stanley, S. V. Buldyrev, G. Franzese, N. Giovambattista, and F. W. Starr, Philos. Trans. R. Soc., A **363**, 509–523 (2005).
[88]R. Horstmann and M. Vogel, J. Chem. Phys. **154**, 054502 (2021).